RSC Advances

PAPER

View Article Online
View Journal | View Issue

Cite this: *RSC Adv.*, 2022, **12**, 7046

A phosphorus-containing imidazole derivative towards the liquid oxygen compatibility and toughness of epoxy resin†

Huihuan Wang,[a] Chuan Li,[b] Zhuang Hou,[a] Bolun Li[a] and Haopeng Cai *[ac]

In order to develop a liquid oxygen-compatible (LOX-compatible) matrix resins for polymer-based fiber-reinforced composites, a novel phosphorus-containing imidazole derivative called VAD containing multifunctional groups was synthesized and used as a co-curing agent for epoxy resin (EP) with simultaneous LOX-compatibility and mechanical improvement. A phosphorus group was introduced into the EP to capture the free radicals generated during the pyrolysis of the polymer to improve LOX compatibility, and the trimethylene group was introduced as a flexible spacer to enhance the toughness of the cured material. In comparison to pure EP, the modified EP with only 2.5 wt% VAD showed excellent mechanical properties with 23.0% and 75.6% increase in tensile and impact strength, respectively. Furthermore, as the content of VAD increased, a thermoset compatible with LOX (according to the liquid oxygen impact test) was obtained, and the flame retardancy was improved (according to the limiting oxygen index test). However, there was no significant sacrifice of transparency or thermal stability. In addition, the LOX compatibility mechanism was analyzed using X-ray photoelectron spectroscopy. As an efficient multi-functional modifier, VAD has a bright future in the modification realm of EP materials.

Received 14th December 2021
Accepted 17th February 2022

DOI: 10.1039/d1ra09049f

rsc.li/rsc-advances

1. Introduction

With the research and development of large launch vehicles, the demand for the lightweight structure of the arrow body is increasing and the structure of the propellant tank is becoming ever more critical. The development of large cryogenic composite tanks with all-composite materials without metal lining has also become an important direction for lightweight arrow structures.[1,2] Compatibility between the polymer matrix and liquid oxygen (LOX) must be solved to develop a composite tank. Epoxy resins (EPs) have found a wide range of applications in low temperature fields due to their excellent mechanical properties, low shrinkage, strong adhesion, moisture resistance, solvent resistance, chemical resistance and corrosion resistance.[3,4] However, when EP is in contact with LOX, it may ignite or trigger a reaction if exposed to external energy, such as friction, collision, mechanical shock, or static electricity.[5] For most EPs, poor LOX compatibility is still a pressing issue. In addition, in the cryogenic environment, the molecular chain of the resin is frozen, the mobility of the resin molecular structure network becomes worse; thus, the brittleness of the resin is intensified, and the impact resistance of the resin reduces substantially, making it difficult to meet the application requirements in a cryogenic environment.[6,7] Therefore, it is necessary to develop modified EPs with prospective LOX compatibility and improved mechanical properties, particularly high fracture toughness.

According to the hot spot theory, when the polymer material is impacted, the mechanical energy in certain local regions (hot spots) is converted to thermal energy to cause local high temperatures, generate free radicals, initiate the chain reaction between polymer and oxygen, and lead to liquid oxygen shock sensitivity.[8] Fundamentally, the incompatible reaction between EP and LOX is essentially consistent with its oxidation and combustion in oxygen. Therefore, the LOX compatibility of EP can be improved by improving its thermal stability and flame retardancy.[9]

Numerous phosphorus-based flame retardants have been utilized for exploiting flame-retardant EPs because of their superior flame-retardant properties, environmental safety, low toxicity, and non-halogen nature. Particularly, 9,10-dihydro-9-oxa-10-phosphaphenanthrene-10-oxide (DOPO) has been widely used in the field of flame retardant because of its strong molecular designability and high reaction activity.[10–12] Given this, DOPO and its derivatives can also enhance the LOX compatibility of EP. LI *et al.* synthesized a new type of epoxy hybrid containing phosphorus/silicon from an epoxy resin containing DOPO and 3-glycidoxy-propyltrimethoxysilane

[a]*School of Materials Science and Engineering, Wuhan University of Technology, Wuhan 430070, China*
[b]*Shanghai Composites Science & Technology Co., Ltd, Shanghai 201112, China*
[c]*Institute of Advanced Materials Manufacturing Equipment and Technology, Wuhan University of Technology, Wuhan 430070, China*

† Electronic supplementary information (ESI) available. See DOI: 10.1039/d1ra09049f

(GLYMO), which achieved compatibility with LOX and possessed significantly enhanced thermal stability.[13] Wu *et al.* utilized DOPO to chemically modify bisphenol A and bisphenol F EP, the LOX compatibility of the modified resin was significantly enhanced, better thermal stability and flame retardancy were also observed.[14]

The introduction of phosphorus-based flame retardants into the EP system can improve its compatibility with LOX. Besides, due to the inferior properties of the phosphorus-containing compounds and the physical blending of the unreacted flame retardant, the other original properties of the EP system deteriorate sharply, especially T_g and mechanical properties.[15,16] The phosphorus flame retardant can achieve an excellent flame retardant effect only when it was grafted onto the cross-linked network.[17,18] Therefore, it is instructive for academic and industrial fields to resolve the contradiction of improving LOX compatibility while maintaining or even improving the mechanical properties of EP by adding a single compound.

The methods to improve the toughness and strength of EP mainly include flexible polymer toughening and nano-material toughening.[19–22] In most cases, EP toughened by nano-materials is prone to phase separation, which reduces the high strength of the matrix and often sacrifices thermal stability, which increases the difficulty of processing.[23,24] The stress relaxation at the crack tip or the strength of the molecular chain is thought to control the fracture toughness of EP at ultra-low temperatures. The degree of cross-linking should be increased to increase the strength of the molecular chain, but the elasticity of the resin will be lost, reducing fracture toughness. For this reason, the epoxy hybrid containing multiple functional groups can be selected, with the rigid chain carrying the load and the flexible chain alleviating stress concentration.

In this work, a phosphorus-containing imidazole derivative VAD whose imidazole ring and phosphophenanthrene group were linked by an aminopropyl chain was designed and synthesized; it can be used as a multifunctional reactive modifier to form a block copolymer with EP. By adjusting the microstructure of EP, flexible segments were introduced in the three-dimensional cross-linking network to improve its molecular flexibility. As a reactive modifier, VAD caused no phase separation during the curing reaction. Whereas, the sacrifice of mechanical properties to increase LOX compatibility was absent. Architecturally, VAD contains a variety of functional groups, phosphophenanthrene as a rigid unit load, long-chain methylene as flexible chain retardation and stress concentration, and a DOPO drape as a flame retardant group. For the purpose of investigating the impact of VAD on the properties of EP matrix, thermal stability, the LOX compatibility, flame retardancy, and mechanical properties of pure and modified EPs were studied and analysed in detail.

2. Results and discussion

2.1 Structural characterization of VAD

FTIR, ^{1}H NMR and ^{31}P NMR studies were conducted to confirm the chemical structure of VAD, and the corresponding results are presented in Fig. 1 and 2.

FTIR spectra of VA, AI, DOPO and VAD are shown in Fig. 1. The stretching vibration absorption peaks of –OH and –CH_3 at 3054 cm^{-1} and 2962 cm^{-1} are derived from VA, the stretching vibration absorption peaks of –CH_2 at 2837 cm^{-1} and 2740 cm^{-1} are derived from AI as well as the characteristic peak of imidazole appearing at 1519 cm^{-1} were observed,[25] while the typical absorption peak of –CHO at 1665 cm^{-1} disappeared in the FTIR spectrum of VAD, indicating the complete reaction between VA and AI. Furthermore, the double peaks of –NH_2 at 3358 cm^{-1} and 3296 cm^{-1} converted to the single peak of –NH at 3399 cm^{-1}, as well as the characteristic peak of P–H at 2436 cm^{-1} from DOPO disappeared, illustrating the nucleophilic addition reaction between the C=N double bond and P–H was substantially completed. Additionally, the absorption peak at 1601, 856, and 756 cm^{-1} are attributed to the benzene ring, and the absorption peaks at 1282 cm^{-1}, 1087 cm^{-1}, 1032 cm^{-1} and 921 cm^{-1} are assigned to the stretching vibrations of P=O, C–N, C–O–C, and P–O–C, respectively. The chemical structure of VAD was validated by the information provided above.

Fig. 2 presents ^{1}H NMR and ^{31}P NMR spectra of VAD. As depicted in Fig. 2(a), a–f corresponds to six types of hydrogen (e, g and h were the same type). 8.7–9.3 ppm belonged to the reactive hydrogen chemical shift of –OH; the chemical shifts of protons, hydrogens of benzene and imidazole groups ranged from 6.7 to 8.2 ppm; 6.6 ppm corresponding to the chemical shift of N–H; 3.8 ppm, 3.7 ppm, 2.3–2.4 ppm and 1.6–1.7 ppm, and were assigned to the He, Hf, Hg and Hh of the alkyl chain, respectively; 3.9–4 ppm was attributed to Hd. Furthermore, the proton peaks' integral area ratio was Ha : Hb : Hc : Hd : H(e + g + h): Hf = 0.9 : 14.2 : 1 : 1.1 : 6 : 3.2, which agreed well with the theoretical value. Two peaks at 30.52 and 33.09 ppm were observed as shown in Fig. 2(b), which were ascribed to the steric hindrance effect of the phosphaphenanthrene group.[26] The results further validated the chemical structure of VAD.

2.2 Morphology analysis

The microstructure of pure EP and EP/VAD thermosets was investigated using SEM and TEM. There was no discernible difference between the two morphologies, as illustrated in Fig. 3(a) and (b), and no phase separation was detected in EP/

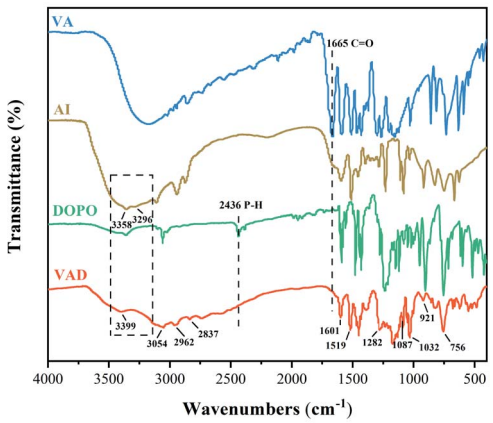

Fig. 1 FTIR spectra of VA, AI, DOPO and VAD.

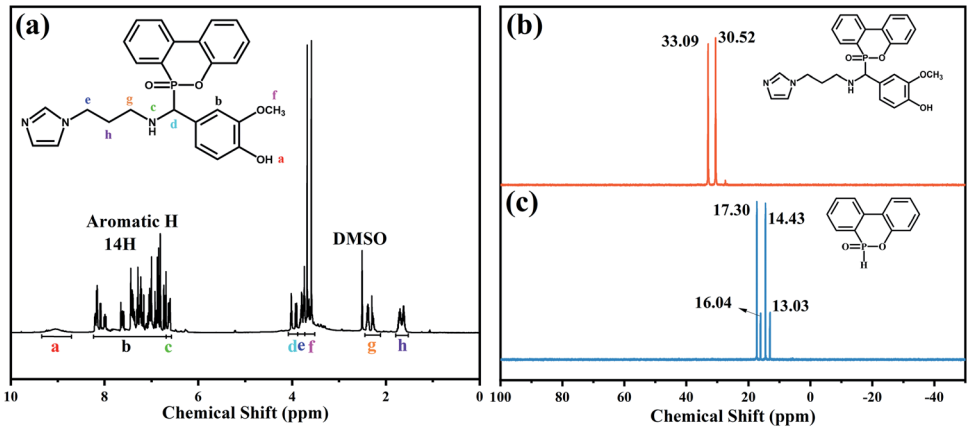

Fig. 2 (a) ^{1}H NMR spectra of VAD; ^{31}P NMR spectra of (b) VAD and (c) DOPO.

VAD-5, indicating that VAD was uniformly distributed in EP and chemically embedded in the cross-linked network of EP, as presented in Fig. 3(d) and 6. The uniform dispersion of VAD in the EP matrix was visually confirmed by SEM-EDX, and element P was uniformly distributed in EP as shown in Fig. 3(c), indicating that VAD was extremely miscible and has no aggregation. All the EP thermosets displayed high transparency, as shown in Fig. 3(e), as a result of the absence of phase separation.

2.3 Curing behavior

Differential scanning calorimetry (DSC) was utilized to investigate the curing behavior of EP mixture. There was just one exothermic peak in each DSC curve as shown in Fig. 4, which corresponded to the curing reaction of EP. The exothermic peak of the EP system was ascribed to the addition reaction of the epoxy group with the amino group. The exothermic peaks of the EP/VAD curing system were ascribed to the ring-opening reaction of amino, imine groups and hydroxyl group with epoxy group and the etherification reaction of imidazole ring with the epoxy group, as shown in Fig. 3(d) of the reaction mechanism of VAD. The feasible crosslinking structural formation of the EP/VAD system is shown in Fig. 6. Furthermore, the exothermic peak temperature of the EP/VAD mixture decreased as the VAD content increased while the exothermic peak temperature of EP/VAD-7.5 was only 157 °C, which was significantly lower than that

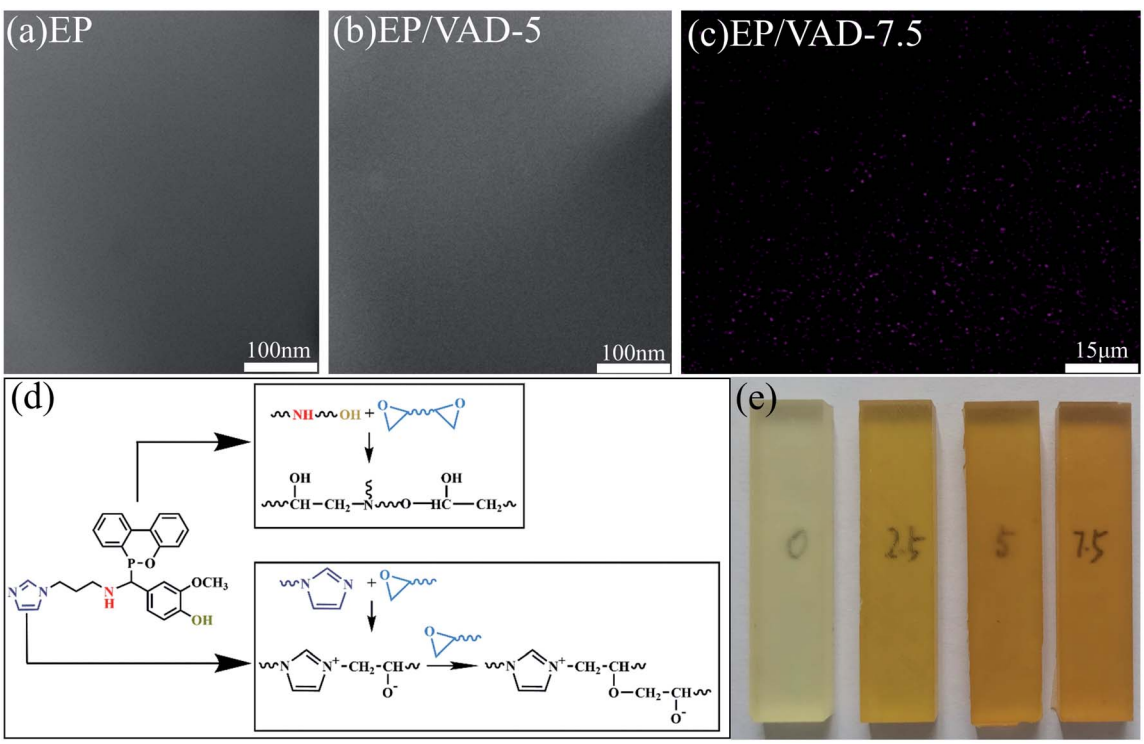

Fig. 3 TEM images of pure EP (a) and EP/VAD-5 (b). (c) P-mapping of EP/VAD-7.5. (d) The reaction mechanism between VAD and EP. (e) Photograph of EP/VAD-*x*.

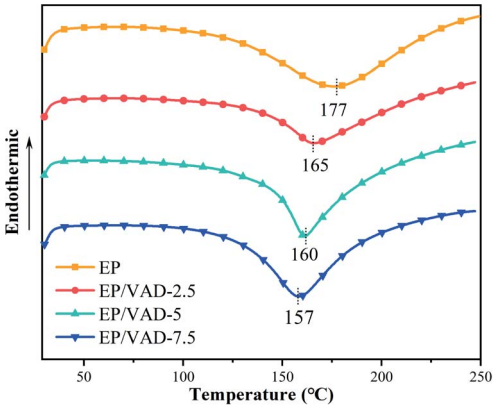

Fig. 4 DSC thermogram of the EP mixtures.

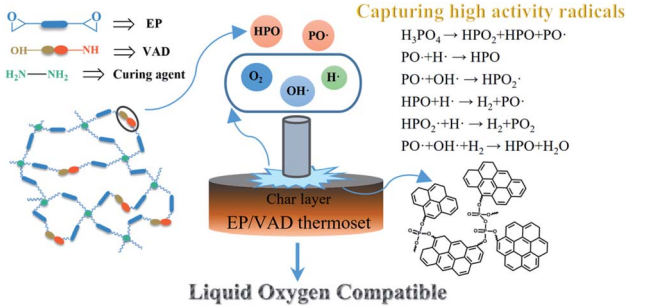

Fig. 6 Liquid oxygen compatibility mechanism of the VAD-modified EP.

of the pure system (177 °C). This behavior was primarily explained by the fact that VAD, as an imidazole curing agent, catalyzed the curing process of EP.[27]

2.4 Thermal stability of EP thermosets

The thermal stability of EP/VAD mixtures was assessed by thermogravimetric analysis (TGA) under N_2 flow. Fig. 5 exhibits the TG and DTG curves, and the detailed data, including the beginning mass loss temperature ($T_{5\%}$), maximum mass loss rate temperature (T_{max}), and carbon residue rate at 800 °C ($CY_{800\ °C}$) are summarized in Table 1. The single-step degradation process for EP/VAD thermosets is shown in Fig. 5(a), which demonstrated a degradation characteristic comparable to pristine EP, indicating that VAD did not affect the main decomposition process of EP. With the content of VAD increasing, $T_{5\%}$ decreased from 359.8 °C to 337.9 °C, and T_{max} decreased from 387.9 °C to 374.1 °C. The decreased thermal stability of P–C and O=P–O bonds in VAD, in compassion with the C–C bond,[28] and the lower crosslinking density in EP/VAD samples (see Table S1 and Fig. S1†), were responsible for the drop of $T_{5\%}$ and T_{max}. In addition, the $CY_{800\ °C}$ increased significantly from 15.9% to 23.6%, indicating that VAD improved the charring ability. It was speculated that the decomposition products of the phosphaphenanthrene group facilitated the char-forming ability of the EP matrix, and imidazolyl groups had good thermal stability, which delayed the thermal degradation of the EP matrix at high temperature.

Table 1 TGA data of the EP/VAD mixture

Samples	$T_{5\%}$ (°C)	T_{max} (°C)	$CY_{800\ °C}$ (%)
EP	359.8	387.9	15.9
EP/VAD-2.5	347.9	381.1	18.2
EP/VAD-5	341.1	378.3	20.2
EP/VAD-7.5	337.9	374.1	23.6

2.5 LOX compatibility and flame retardancy analysis

LOX compatibility of all samples were determined using the LOX mechanical impact test. Impact reaction sensitivity (IRS) of the samples was calculated according to the following formula (1):[29]

$$IRS = \frac{\sum_{i}^{4} w_i n_i}{N} \quad (1)$$

where N represents the number of tests; w_i are the weighted coefficients, where w_1 (burning) = 1, w_2 (explosion) = 0.9, w_3

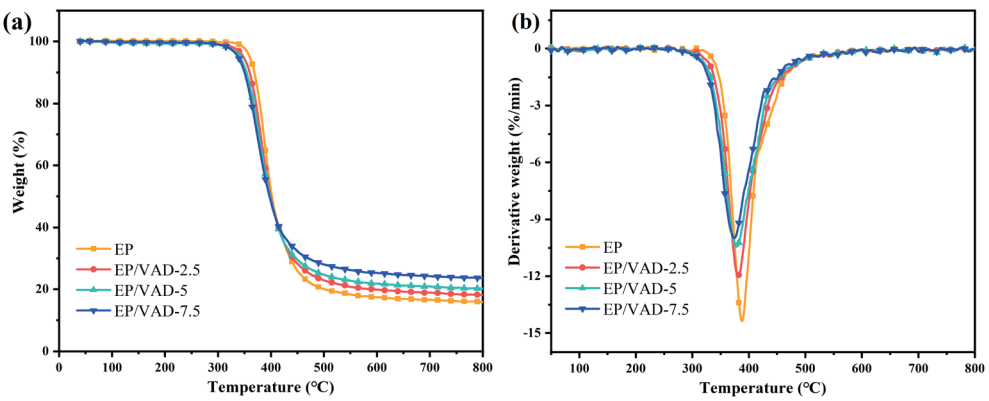

Fig. 5 (a) TG curves of the EP/VAD mixture. (b) DTG curves of the EP/VAD mixture.

Table 2 The reaction and IRS of resin systems in the LOX impact test

	Liquid oxygen incompatibility					
Sample	Burning	Explosion	Flash	Charring	IRS (%)	LOI (%)
EP	0	2	6	0	27	25.6
EP/VAD-2.5	0	1	0	4	12.5	29.5
EP/VAD-5	0	0	1	1	5	30.6
EP/VAD-7.5	0	0	0	0	0	31.2

(flash) = 0.6, w_4 (charring) = 0.4; n_i are the frequencies of LOX incompatibility phenomena. The lower the IRS, the better the LOX compatibility of the material, and the IRS value of the LOX tank should not be greater than 5%. Besides, the limited oxygen index (LOI) was conducted to evaluate the relationship between flame retardancy and LOX compatibility of EP samples. The IRS and LOI values of all systems are displayed in Table 2.

As the content of VAD increased, the IRS of EP/VAD thermosets showed a downward tendency from 27% to 0% while the LOI value had an obvious increase from 25.6% to 31.2% as presented in Table 2, indicating that flame retardant element P can improve the LOX compatibility of EP. Moreover, during the 20 times of impact tests, there was no reaction detected for EP/VAD-7.5, demonstrating that EP/VAD-7.5 were compatible with LOX.

Combined with the above thermal stability analysis, the LOX impact test and the limiting oxygen index test results, the corresponding LOX compatibility mechanism is shown in Fig. 6. When EP sample was impacted by high energy in LOX, the mechanical energy was converted into thermal energy to decompose the hot spot area of the resin, and the H·, O·, and OH· high-energy free radicals were generated, which caused chain decomposition of the resin and lead to incompatible reactions.[30] However, for EP modified by VAD, a large number of PO· and HPO_2· free radicals were released during thermal degradation can capture these high energy free radicals, thus inhibiting the impact-sensitive reaction between EP and LOX.

By observing the micro-morphology of the EP/VAD-5 sample after the LOX impact test, a thin deposited carbon layer was observed on the surface of the failed sample (see Fig. S2†), which inhibited the further combustion of the polymer and prevented the occurrence of LOX incompatibility. Further analysis was shown in Chapter 2.6.

2.6 Analysis of the surface elements after the impact test

XPS measurement was utilized to determine the surface elements of EP samples after the impact test, and research the effect of P on improving the compatibility between LOX with EP. The detailed contents of elements, including P, C, N, O and O/C ratios, were summarized in Table 3.

Generally, during the pyrolysis under the O_2 atmosphere, EPs are oxidized firstly and subsequently carbonized. The oxidation denotes an increased O/C ratio, while the carbonization suggests decreased O/C ratio. The reaction between EPs and LOX during the impact test can be explained by this mechanism.[13] As presented in Table 3, after the impact test, the O/C ratio of pure EP decreased, indicating that it was carbonized during the impact test; the increased O/C ratio of EP/VAD-5 indicated that oxidation appeared during the impact test. It revealed that the neat EP had poor LOX compatibility, while EP/VAD-5 showed better LOX compatibility. This behavior was consistent with the results that EP samples were impacted in LOX.

Table 3 Elemental contents of the EP specimens before and after liquid oxygen impact

		Element content (%)				
Specimen	The impact test	P	C	N	O	O/C
EP	Before	—	75.43	8.29	16.28	0.2158
	After (no reaction)	—	75.9	8.52	15.58	0.2053
	After (explosion)	—	76.8	8.84	14.36	0.1869
EP/VAD-5	Before	0.36	79.75	3.93	15.96	0.2001
	After (no reaction)	0.4	78.93	3.55	17.11	0.2168
	After (flash)	0.87	78.05	4.59	16.49	0.2113

The P_{2p} spectra of EP/VAD-5 before and after the impact test are presented in Fig. 7. The spectrum before the impact test consisted of P–C and O=P–O bonds and was decided from the primary chemical structure of EP/VAD. Compared with samples before the impact test, the P_{2p} peak of the unreacted samples after the impact test was slightly wider, indicating the formation of PO_3 groups; the P_{2p} peak of the samples with the reaction after the impact test shifted significantly to higher binding energy, and its strength raised obviously, revealing that the phosphorus-containing groups in EP/VAD samples were heated to decompose into a large number of PO_3 groups existing in the form of polymetaphosphoric acid to prevent further combustion of EP. The above results showed that the flame retardant mechanism of organophosphorus compounds in the condensed phase was that the generated polymetaphosphoric acid facilitated the formation of compact and stable phosphorus-rich char layer, which hindered availably of the diffusion of oxygen into the combustion and prevented the polymer from further combustion, as shown in Fig. 6.

Table 3 also shows that P and O contents of samples after combustion are significantly higher than those before impact, which further proved the above conclusion.

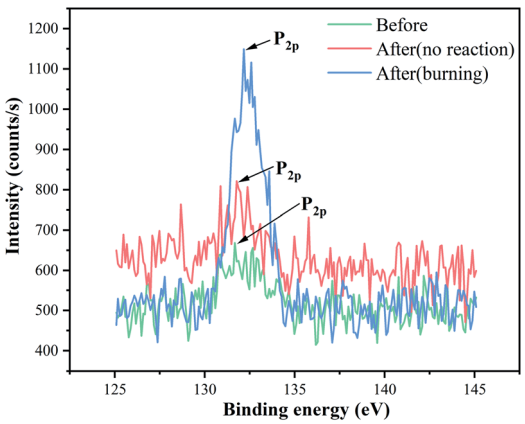

Fig. 7 P_{2p} spectra of EP/VAD-5 before and after LOX impact.

Table 4 Mechanical properties of the EP samples

Sample	Elastic modulus (MPa)	Tensile strength (MPa)	Flexural modulus (MPa)	Flexural strength (MPa)	Elongation at break (%)	K_{IC} (MPa m$^{-1/2}$)	Impact strength (KJ m^{-2})
EP	2378.1 ± 45	65.6 ± 1.5	2947.8 ± 9.6	93.6 ± 0.1	3.66 ± 0.05	1.97 ± 0.12	18.39 ± 1.2
EP/VAD-2.5	2957.7 ± 51	80.7 ± 1.3	2963.0 ± 27.2	94.5 ± 0.5	6.38 ± 0.04	3.52 ± 0.09	30.51 ± 0.9
EP/VAD-5	2971.6 ± 44	70.1 ± 1.9	3060.7 ± 32.1	100.7 ± 0.7	3.75 ± 0.05	2.82 ± 0.13	25.78 ± 1.0
EP/VAD-7.5	3150.0 ± 53	66.0 ± 1.7	3214.6 ± 32.6	108.3 ± 0.7	3.11 ± 0.06	2.31 ± 0.15	19.91 ± 1.4

2.7 Mechanical performance analysis

In general, in most flame retardant systems, excellent mechanical properties are usually mutually exclusive with high flame retardancy, which means the increase of one performance usually brings about the sacrifice of the other. Hence, the influence of VAD on the mechanical properties of EP were investigated, including impact strength, critical stress intensity factor (K_{IC}), tensile strength, elastic modulus, flexural strength and modulus, as shown in Table 4. The K_{IC} value of fracture toughness was calculated using the following formula:

$$K_{IC} = \frac{P_m S}{DW^{3/2}} f\left(\frac{a}{w}\right) \quad (2)$$

$$f\left(\frac{a}{w}\right) = \frac{3\left(\frac{a}{w}\right)^{\frac{1}{2}}\left[1.99 - \frac{a}{w}\left(1-\frac{a}{w}\right)\left(2.15 - 3.93\frac{a}{w}\right) + 2.7\left(\frac{a}{w}\right)^2\right]}{2\left(1+2\frac{a}{w}\right)\left(1-\frac{a}{w}\right)^{\frac{3}{2}}} \quad (3)$$

where P_m represents the maximum load during failure, S is the span (32 mm), D is the thickness of the specimen, W expresses the width of the specimen, and a represents the length of the prefabricated crack.

The addition of a small amount of VAD to the matrix can improve both strength and toughness. As shown in Table 4 and Fig. 8, EP/VAD samples exhibited greater tensile strength (80.7–66 MPa) and elastic modulus (2957.7–3150 MPa), compared with those of pure EP (65.5 MPa and 2378.1 MPa). Similar phenomena were detected in flexural strength and modulus. The improvement in tensile and flexural properties can be attributed to (1) the addition of VAD and the introduction of a large number of rigid benzene rings in the EP matrix, and (2) many hydroxyl groups in the epoxy main chain can form hydrogen bonds with imidazole rings, enhancing the intermolecular interaction.[31]

Furthermore, the impact strength, elongation at break and K_{IC} of EP-VAD-2.5 increased greatly, reaching the highest value of 30.51 kJ m^{-2}, 6.38% and 3.52 MPa m$^{-1/2}$, respectively, and then decreased linearly with the increase of VAD content, which attributed to internal defects in the homogeneous system, and lead to the early failure of the material.

The specific toughening mode of VAD on EP thermosets can be explained according to the morphology of the fracture surface examined by SEM, as presented in Fig. 9. As a result of the lack of energy dissipation, pure EP showed a characteristic brittle section with a "radial" pattern indicating that the crack propagates rapidly as shown in Fig. 9(a). Whereas EP/VAD samples (Fig. 9(b) and (c)) manifested the "dimple-like" ductile fracture characteristics,[19] a significant increase in ripples and folds was observed, certifying that the crack deflection inhibited the rapid fracture of the sample. The relatively large number of cracks and rougher fracture surfaces signified expanded fracture area and complex fracture paths, which were believed to dissipate more energy and thus improve toughness.[32] The remarkable strengthening and toughening effect of VAD was related to the non-phase separation morphology and the perfect combination of rigid and flexible groups. Firstly, the formation of block copolymers of VAD and EP can improve the energy dissipation in the failure process, and the introduction of plentiful aromatic rings, which can generate π–π interaction with the matrix further improved the interaction between VAD and the matrix.[33] Secondly, the flexible

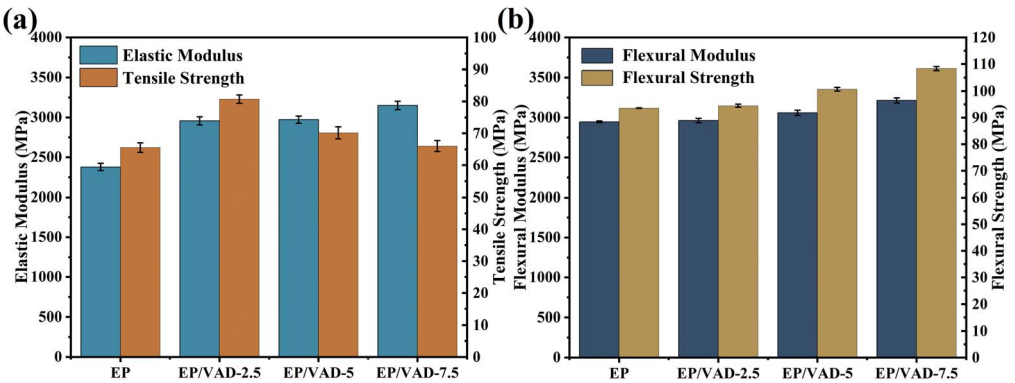

Fig. 8 (a) Tensile strength-elastic modulus diagram (b) flexural strength-flexural modulus diagram.

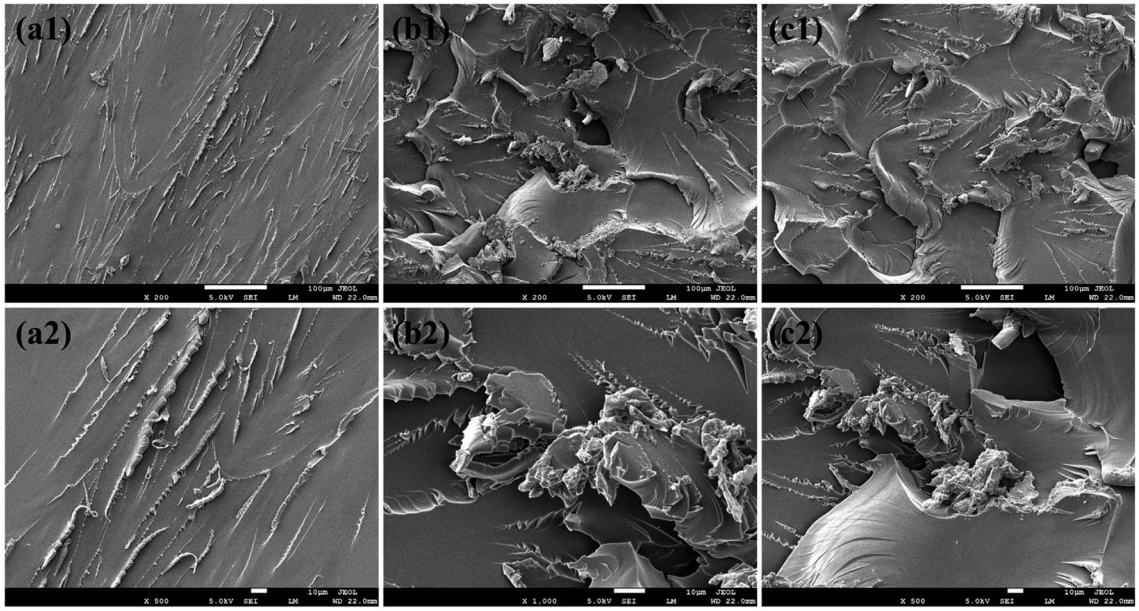

Fig. 9 SEM images of the fracture surfaces of the samples: (a) pure EP, (b) EP/VAD-2.5 and (c) EP/VAD-5 at different magnification.

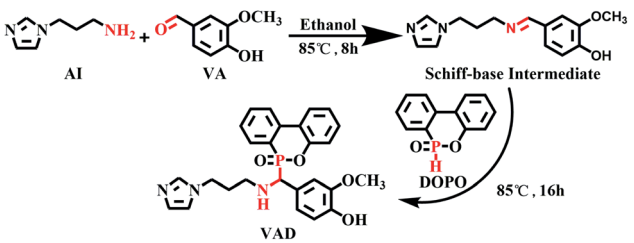

Scheme 1 Synthesis of the multi-functional modifier VAD.

chain of VAD increased the movement ability between molecular segments, increasing the likelihood of homogeneous shear deformation and dissipating more fracture energy *via* intermolecular motion. Therefore, VAD played a toughening effect in the mode of energy absorption described as "*in situ* toughening".[34]

3. Experimental

3.1 Materials

1-(3-Aminopropyl)-imidazole (AI, ≥98% purity) was obtained from Shanghai Baishun Biological Technology Co., Ltd Vanillin (VA, 99% purity) and 9,10-dihydro-9-oxa-10-phosphaphenanthrene-10-oxide (DOPO, 97% purity) were obtained from Shanghai Macleans Biochemical Technology Co., Ltd (China). Anhydrous ethanol and toluene were obtained from Sinopharm Chemical Reagent Co., Ltd. Bisphenol F epoxy resin (EP, epoxide equivalent weight: ~158–172 g per equiv.) was purchased from Royal Dutch Shell. The amine curing agent (MACA) is a mixture of diethyl toluene diamine (DETDA), diaminodiphenylmethane (DDM) and isophorone diamine (IPDA) at a ratio of 10 : 2 : 3. They were purchased from Shanghai Demao Chemical Co., Ltd, Wanhua Chemical Group Co., Ltd, and Shanghai Aladdin Company (China), respectively. Unless otherwise specified, all commercially available materials were used in accordance with the standards received.

Table 5 Formulas of the EP thermosets

Samples	EP (g)	MACA (g)	VAD (g)	P (wt%)
EP	100	26.50	0	0
EP/VAD-2.5	100	25.85	3.23	0.15
EP/VAD-5	100	25.21	6.59	0.30
EP/VAD-7.5	100	24.55	10.09	0.45

3.2 Synthesis of VAD

The structural formula of VAD is presented in Scheme 1. At room temperature, anhydrous ethanol (100 mL) and vanillin (12.17 g, 0.08 mol) were added to a 250 mL three-neck flask equipped with a reflux condenser, mechanical agitator, and dripping funnel. After the VA was completely dissolved, AI (10.01 g, 0.08 mol) was dripped into the flask, the mixture was gradually heated to 85 °C, and the temperature was maintained for 8 hours while stirring continuously. Next, DOPO (17.28 g, 0.08 mol) was added to the flask, and the admixture was refluxed and stirred for 16 h. Finally, the mixture was spun to remove the solvent, followed by 12 hours of drying in a vacuum oven at 70 °C. The pale-yellow powder was finally obtained (yield: 85%).

3.3 Preparation of EP thermosets

The EP modified with different VAD content was called EP/VAD-*x*. Table 5 showed the specific formulas of EP thermosets. The following experimental approach was used to prepare all EP

samples. First, a homogenous mixture of EP and VAD was prepared in a glass flask at 70 °C using a mechanical stirrer. A stoichiometric quantity of MACA was added, and the mixture was continuously agitated at 70 °C for 10 minutes before being degassed under a vacuum. Afterwards, the aforesaid mixture was poured into a preheated mould and cured at 90 °C for 2 h, 110 °C for 2 h, and 150 °C for 5 h of post-curing. After naturally cooling to room temperature, the EP/VAD-*x* samples were obtained. As a comparison, pure EP was prepared using the same method. For all systems, the total amount of active protons in VAD and MACA equals the number of epoxy groups in EP.

3.4 Characterization

Fourier transform infrared (FTIR) spectrum was measured using potassium bromide discs at the range of 4000–400 cm^{-1} using a Nicolet 6700 infrared spectrometer, America.

^{1}H NMR and ^{31}P NMR spectra were acquired, using DMSO-d_6 as the solvent, using an NMR spectrometer, Bruker AV400, Switzerland.

Transmission electron microscopy (TEM) of samples was carried out using a transmission electron microscope (JEM-1400Plus, Japan) at 120 kV. Scanning electron microscopy (SEM) was utilized to acquire the fracture morphology of the tensile specimen and the failed surface micro-morphology caused by the impact with LOX using a scanning electron microscope (JSM-7500F, Japan) under the activation voltage of 20 kV. An energy-dispersive X-ray spectrometer (EDX) was fitted for the P element investigation in the surface scanning model.

Differential scanning calorimetry (DSC) measurement (heating rate = 10 °C min^{-1}, 30–250 °C, N_2 atmosphere) was performed using a PerkinElmer DSC 4000 instrument, USA.

Thermogravimetric analysis (TGA) was performed using a NETZSCH STA449F3 instrument, Germany (heating rate = 10 °C min^{-1}, 30–800 °C, N_2 atmosphere).

The LOX compatibility was tested under 98 J impact energy using the Army Ballistic Missile Agency (ABMA)-type impact tester according to ASTM D2512-95.[35] A specimen of the test material, whose dimension was 20 mm in diameter and 2 mm thick, was placed in a specimen cup, pre-cooled with LOX for 10 min. The 10 kg hammer was released from a height of 1 meter, which transmitted 98 J energy to the test sample. According to whether any LOX-impact sensitive response (burning, explosion, flash or charring) occurred during the test and the number of sensitive phenomena was used to characterize the impact reaction sensitivity (IRS). A material subjected to 20 impact tests with no response would be considered compatible with LOX.

The limited oxygen index (LOI) values were determined using an ASTM D2863-compliant JF-3 oxygen index meter (Jiangning, China), and all samples were 100 × 6.5 × 3 mm^3.

X-ray photoelectron spectroscopy (XPS) technique was used to measure the surface element compositions at 100–1400 eV of the cured EPs before and after the LOX impact using X-ray photoelectron spectroscopy, ESCALAB 250Xi instrument, USA.

Tensile and flexural properties were conducted according to GB/T 2567–2008 using a universal testing machine (Instron 5967, USA) at a 2 mm min^{-1} loading rate; the impact strength was executed on a pendulum impact tester (XJJD-50, China). Critical stress intensity factors (K_{IC}) were assessed using a universal testing machine (SHT4106, USA) in the three-point bending test at a 1 mm min^{-1} loading rate according to ASTM D5045-14. The sample dimension was 35.2 × 8 × 4 mm^3 and the length of the prefabricated crack was 3.6 mm. Each of the above tests went through five parallel tests, and the obtained value was the average of the five tests.

4. Conclusion

The challenge of developing high-performance thermosetting EP with both LOX compatibility and enhanced mechanical properties at the same time by adding a single compound remains. To cater to the requirement of the LOX environment, a new type of phosphorus-containing imidazole molecule (VAD) was successfully designed and used as a multi-functional additive to vest thermosetting EP with desired LOX compatibility, ideal toughening and strengthening properties. The morphology analysis indicated that VAD was uniformly dispersed in the EP matrix, and a homogeneous system was formed. The DSC measurement determined that VAD participated in the curing process and expedited the crosslinking reaction due to the catalysis of the imidazole ring. Compared with pure EP, the obtained EP/VAD-2.5 showed excellent mechanical properties with 23.0%, 75.6% and 78.7% increase in tensile strength, impact strength and K_{IC}, respectively. Additionally, when the VAD content was 7.5 wt%, the compatibility of EP with LOX was realized, and the flame retardancy was greatly improved as evidenced by the IRS of EP thermosets decreasing from 29% to 0%, and LOI increasing from 25.6% to 31.2%. At the same time, these improvements did not sacrifice the transparency or thermal stability of the obtained materials. With these characteristics, EP/VAD system holds appealing prospective applications in cryogenic areas.

Author contributions

Huihuan Wang: conceived the idea of this study, designed the experiment, carried on the sample synthesis and the test characterization. Chuan Li: carried on the liquid oxygen impact test. Huihuan Wang, Chuan Li, Zhuang Hou, Bolun Li, and Haopeng Cai analyzed and discussed the data. Huihuan wang and Haopeng Cai co-wrote and revised the manuscript.

Conflicts of interest

The authors declare that they have no known competing financial interests or personal relationships that could have appeared to influence the work reported in this paper.

Acknowledgements

This work was supported by the National Key R&D Program of China (2020YFA0711700) and the National Foundation of China (Grant No. 2019-JCJQ-ZD-042-00).

Notes and references

1 N. Liu, B. Ma, F. Liu, W. Huang, B. Xu, L. Qu and Y. Yang, *Composites, Part A*, 2021, **143**, 106297.
2 X. H. Shi, L. Chen, Q. Zhao, J. W. Long, Y. M. Li and Y. Z. Wang, *Compos. Sci. Technol.*, 2020, **187**, 107945.
3 S. Q. Huo, P. A. Song, B. Yu, S. Ran, V. S. Chevali, L. Liu, Z. Fang and H. Wang, *Prog. Polym. Sci.*, 2021, **114**, 101366.
4 X. Y. Dai, P. H. Li, Y. L. Sui and C. L. Zhang, *Eur. Polym. J.*, 2021, **147**, 110319.
5 G. Wang, X. Li, R. Yan and S. Xing, *Mater. Sci. Eng., B*, 2006, **132**, 70–73.
6 X. F. Yi, A. K. Mishra, N. H. Kim, B. Ku and J. H. Lee, *Composites, Part A*, 2013, **49**, 58–67.
7 B. C. Kim, S. W. Park and D. G. Lee, *Compos. Struct.*, 2008, **86**, 69–77.
8 F. P. Bowden and A. D. Yoffe, *Am. J. Phys.*, 1952, **20**, 250.
9 T. Mill, D. L. Chamberlain, R. S. Stringham, N. A. Kirshen and K. C. Irwin, *Report*, NASA, USA, 1970.
10 Y. F. Ai, L. Xia, F. Q. Pang, Y. L. Xu and R. K. Jian, *Composites, Part B*, 2020, **193**, 108019.
11 W. Xie, S. Huang, D. Tang, S. Liu and J. Zhao, *RSC Adv.*, 2020, **10**, 956–1965.
12 H. Luo, W. Rao, Y. Liu, P. Zhao, L. Wang and C. Yu, *J. Appl. Polym. Sci.*, 2020, **137**, 49427.
13 J. Li, Z. Li, H. Wang, Z. Wu, Z. Wang and S. Li, *RSC Adv.*, 2016, **6**, 9112–9123.
14 Z. Wu, J. Li and Z. Wang, *Polym. Adv. Technol.*, 2015, **26**, 153–159.
15 G. Wang and Z. Nie, *Polym. Degrad. Stab.*, 2016, **130**, 143–154.
16 G. You, Z. Cheng, Y. Tang and H. He, *Ind. Eng. Chem. Res.*, 2015, **54**, 7309–7319.
17 S. Yang, J. Wang, S. Huo, M. Mei and J. Wang, *Polym. Degrad. Stab.*, 2015, **121**, 398–406.
18 K. A. Salmeia and S. Gaan, *Polym. Degrad. Stab.*, 2015, **113**, 119–134.
19 T. Liu, Y. Nie, R. Chen, L. Zhang, Y. Meng and X. Li, *J. Mater. Chem. A*, 2015, **3**, 1188–1198.
20 K. Mimura, H. Ito and H. Fujioka, *Polymer*, 2001, **42**, 9223–9233.
21 W. Liu, R. Zhou, H. L. S. Goh, S. Huang and X. Lu, *ACS Appl. Mater. Interfaces*, 2014, **6**, 5810–5817.
22 S. H. Lim, K. Y. Zeng and C. B. He, *Mater. Sci. Eng., A*, 2010, **527**, 5670–5676.
23 M. A. EL-Hadek, *Metall. Mater. Trans. A*, 2014, **45**, 317–323.
24 D. Ratna, O. Becker, R. Krishnamurthy, G. P. Simon and R. J. Varley, *Polymer*, 2003, **44**, 7449–7457.
25 W. Liu, K. L. Koh, J. Lu, L. Yang, S. Phua, J. Kong, Z. Chen and X. Lu, *J. Mater. Chem.*, 2012, **22**, 18395.
26 S. Huo, J. Wang, S. Yang, C. Li, X. Wang and H. Cai, *Polym. Degrad. Stab.*, 2019, **159**, 79–89.
27 S. Yang, Q. Zhang, Y. Hu, G. Ding, J. Wang, S. Huo, B. Zhang and J. Chen, *Mater. Lett.*, 2018, **216**, 127–130.
28 S. Yang, J. Wang, S. Huo, M. Wang and L. Cheng, *Ind. Eng. Chem. Res.*, 2015, **54**, 7777–7786.
29 R. L. Hauser and W. F. Rumpel, *Adv. Cryog. Eng.*, 1963, **8**, 242–247.
30 B. Schartel, *Materials*, 2010, **3**, 4710–4745.
31 J. Jia, X. Sun, X. Lin, X. Shen, Y. W. Mai and J. K. Kim, *ACS Nano*, 2014, **8**, 5774–5783.
32 X. F. Liu, B. W. Liu, X. Luo, D. M. Guo, H. Y. Zhong, L. Chen and Y. Z. Wang, *Chem. Eng. J.*, 2020, **380**, 122471.
33 Y. Qiu, L. Qian, H. Feng, S. Jin and J. Hao, *Macromolecules*, 2018, **51**, 9992–10002.
34 D. Zhang and D. Jia, *J. Appl. Polym. Sci.*, 2006, **101**, 2504–2511.
35 R. Y. Kim, C. W. Lee, J. Camping, and K. B. Bowman, *46th Aiaa/ASME/ASCE/AHS/ASC Structures, Structural Dynamics & Materials Conference*, Austin, April 2005.